Computer Modeling in Engineering & Sciences
DOI:10.32604/cmes.2020.08270
Article

Three-Dimensional Collapse Analysis for a Shallow Cavity in Layered Strata Based on Upper Bound Theorem

Hongtao Wang[1,2,*], Ping Liu[1,2], Lige Wang[3,4,*], Chi Liu[5], Xin Zhang[1,2] and Luyao Liu[1,2]

[1]School of Civil Engineering, Shandong Jianzhu University, Jinan, China
[2]Key Laboratory of Building Structural Retrofitting and Underground Space Engineering (Shandong Jianzhu University), Ministry of Education, Jinan, China
[3]Department of Chemical and Biological Engineering, University of Sheffield, Sheffield, UK
[4]State Key Laboratory of Geomechanics and Geotechnical Engineering, Institute of Rock and Soil Mechanics, Chinese Academy of Sciences, Wuhan, China
[5]Jinan Rail Transit Group Co., Ltd., Jinan, China
*Corresponding Authors: Hongtao Wang. Email: wanghongtao918@163.com; Lige Wang. Email: L.G.Wang@psenterprise.com
Received: 11 August 2019; Accepted: 25 March 2020

Abstract: Layered rock strata are observed to be common during the excavation of tunnels or cavities, and may significantly affect the deformation and failure characteristics of surrounding rock masses due to various complex forms and mechanical properties. In this paper, we propose a three-dimensional axisymmetric velocity field for roof collapse of shallow cavities in multi rock layers, by considering the influences of roof cross-section shapes, supporting pressure, ground overload, etc. The internal energy dissipation rate and work rates of external forces corresponding to the velocity field are computed by employing the Hoek-Brown strength criterion and its associated flow rule. Further, the equations of the collapse surfaces and the corresponding weight of collapsing rock masses are derived on the basis of upper bound theorem. Furthermore, we validate the proposed method by comparing the results of numerical calculations and existing research findings. The change laws of the collapse range under varying parameters are obtained for the presence of rectangular and spherical cavities. We also find that the three-dimensional mechanism is relatively safer for engineering designing actually, compared with the traditional two-dimensional mechanism. All these conclusions may provide workable guidelines for the support design of shallow cavities in layered rock strata practically.

Keywords: Shallow cavity; three-dimensional collapse; layered rock strata; upper bound theorem; Hoek-Brown strength criterion

1 Introduction

As urban modernization accelerates, traffic congestion, environment pollution, land shortage and other problems in urban area have become increasingly prominent. In this context, it becomes an inevitable trend for urban development in the world to build subways, underground shopping malls, utility tunnels, underground energy facilities and other various underground buildings by exploiting underground space.

However, since such projects are generally buried shallow, the ground settlement may be inevitable in excavation process, and adverse control on it may even lead to surface collapse at times, threatening the public's life and property.

The stability of tunnel or cavity is a hotspot for many scholars. Among numerous analytical approaches, the upper bound method has gained great recognitions and extensive applications [1–11]. In this method, a velocity field that satisfies the failure characteristics of tunnel or cavity is required to be built in advance, and the stress equilibrium conditions inside rocks or soils can be neglected in some cases. By doing so, the complex and tedious calculation can be simplified effectively. Then a close-to-actual failure mechanism can be obtained based on virtual work principle. Due to the above advantages, some scholars had utilized this method to investigate the roof collapse mechanisms of tunnels or cavities in recent years. Initially, Fraldi et al. [12–14] introduced the Hoek-Brown failure criterion into this method to investigate the collapse characteristics of deep tunnel roof, which provides a theoretical basis for later research works. Recently, Fraldi et al. [15] proposed a general characterization of tunnels depth based on the profundity of the excavation and on the variability of the rock mass mechanical parameters, and analyzed the collapse characteristics of intermediate tunnels. Based on their method, Huang et al. [16] constructed the collapse mechanism for deep circular tunnels, and obtained the effects of some factors, such as tunnel diameter, pore water pressure and etc. on roof collapse region. Zhang et al. [17] conducted upper bound limit analysis on a deep circular tunnel, and proposed a judging criterion to distinguish whether the roof collapses of deep tunnels will occur or not. Further, Yang et al. [18,19] developed the two-dimensional collapse mechanisms to three-dimensional cases, and obtained the three-dimensional collapse characteristics for spherical cavities and rectangular cavities. Guan et al. [20] proposed a three-dimensional collapse mode for a supported cavity roof with arbitrary profile, and obtained the stability graph with respect to roof profile and cavity span. In these research woks, the roof rock masses or soil masses are assumed to be homogeneous generally.

It should be noted that layered rock masses are observed to be common during the excavation of cavities or tunnels due to the influence of diagenetic environment or process in strata. Compared with the homogeneous strata, layered strata present with apparent non-homogeneity and anisotropy, and the various complex forms and mechanical properties may significantly affect the deformation and failure characteristics of cavity or tunnel surrounding rock masses. To solve this problem, Qin et al. [21,22] and Yang et al. [23,24] incorporated the stratification and non-homogeneity characteristics of rock masses or soil masses into two-dimensional collapse analysis of deep tunnels. Similarly, they [25–27] also incorporated this influence into the three-dimensional roof collapse mechanisms.

All above-mentioned research works on roof stability are limited to deep tunnels or cavities only. In the field of shallow tunnel collapse, Yang et al. [28] proposed the collapse mechanism for a shallow circular tunnel. Yang et al. [29] conducted upper bound limit analysis on roof collapse for a shallow tunnel in two-layered rock strata. Wang et al. [30,31] proposed two kinds of collapse mechanisms for a shallow tunnel by incorporating the effects of changing groundwater table and pore water pressure. Lyu et al. [32] investigated the collapse of shallow tunnels in inclined rock stratum. These are some representative research works, but the collapse mechanisms in these works are assumed to be two-dimensional on the basis of plane strain hypothesis.

As for shallow cavities, such as spherical or rectangular cavities, the corresponding collapse surfaces may easily reach to ground surface, and cannot be simplified to two-dimensional modes. Moreover, many other factors, such as profile shape, layered rock masses and etc. may have significant influence on cavity stability. However, the collapse characteristics for a shallow cavity in layered strata have not been well investigated in present. Based on existing research works, we propose an axisymmetric roof collapse mechanism for a shallow cavity in layered rock strata in this paper. The equations of the collapse surfaces and the corresponding weight of collapsing rock masses are derived using upper bound theorem and

variation principle. The change laws of the collapse mechanisms under varying parameters are investigated for the presence of rectangular and spherical cavities. The results may provide theoretical guidance for design and construction of shallow cavities.

2 Hoek-Brown Strength Criterion and Its Associated Flow Rule

The Hoek-Brown strength criterion [33–35] has been widely applied in geotechnical engineering. The strength envelope corresponding to this criterion is a curve (Fig. 1), which can effectively describe the non-linear failure characteristics of rock masses. In the Mohr plane $\sigma_n - \tau_n$, the expression can be written as follows [12]:

$$\tau_{\mathrm{n}} = A\sigma_{\mathrm{c}}\left[(\sigma_{\mathrm{n}} + \sigma_{\mathrm{t}})\sigma_{\mathrm{c}}^{-1}\right]^{B} \tag{1}$$

where A and B are two dimensionless empirical parameters related to rock property; σ_c refers to the rock compressive strength; σ_t refers to the rock tensile strength. Under the circumstance where the rock cohesion and internal friction angle are respectively expressed as c and φ, by setting $B = 1$, $A = \tan\varphi$ and $\sigma_{\mathrm{t}} = c(\tan\varphi)^{-1}$, the Hoek-Brown strength criterion can be converted to the well-known Mohr-Coulomb strength criterion.

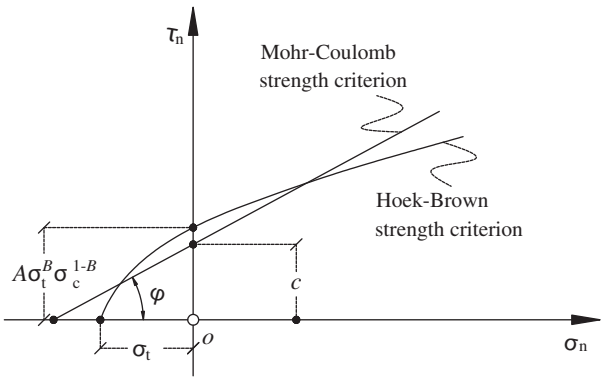

Figure 1: Hoek-Brown strength criterion

In accordance with the traditional plasticity theory and the associated flow rule, we assume that the yield function F ($F = \tau_n - A\sigma_c\left[(\sigma_n + \sigma_t)\sigma_c^{-1}\right]^B$) for rock failure in the Mohr plane $\sigma_n - \tau_n$ coincides with the corresponding potential function Q. Then an incremental constitutive relation listed as follows can be established by using the potential theory [36]:

$$\dot{\epsilon}_{ij} = \dot{\lambda}\frac{\partial Q}{\partial \sigma_{ij}} = \dot{\lambda}\frac{\partial F}{\partial \sigma_{ij}} \tag{2}$$

where $\dot{\lambda}$ refers to a plasticity factor; $\dot{\epsilon}_{ij}$ to the plasticity strain rate component; and σ_{ij} to the stress component. By utilizing the Hoek-Brown strength criterion and the associated flow rule, the roof failure characteristics for shallow cavities are investigated in this paper using upper bound method.

3 Three-Dimensional Axisymmetric Collapse Mechanism for a Shallow Cavity in Layered Strata

In most cases, the shallow cavities are more liable to collapse than the deep cavities. One important reason is that the self-bearing arch structure inside the roof surrounding rock masses may be more difficult to form when the thickness of the overlaying rock is smaller. Thus the roof failure in shallow cavities frequently reaches to the ground surface. Based on this characteristic, we propose a three-dimensional kinematically admissible velocity field for roof collapse in a shallow cavity in n-layered strata, as shown in Fig. 2. Wherein, H is the burial depth of the cavity, p_a is the ground overload, and p_s

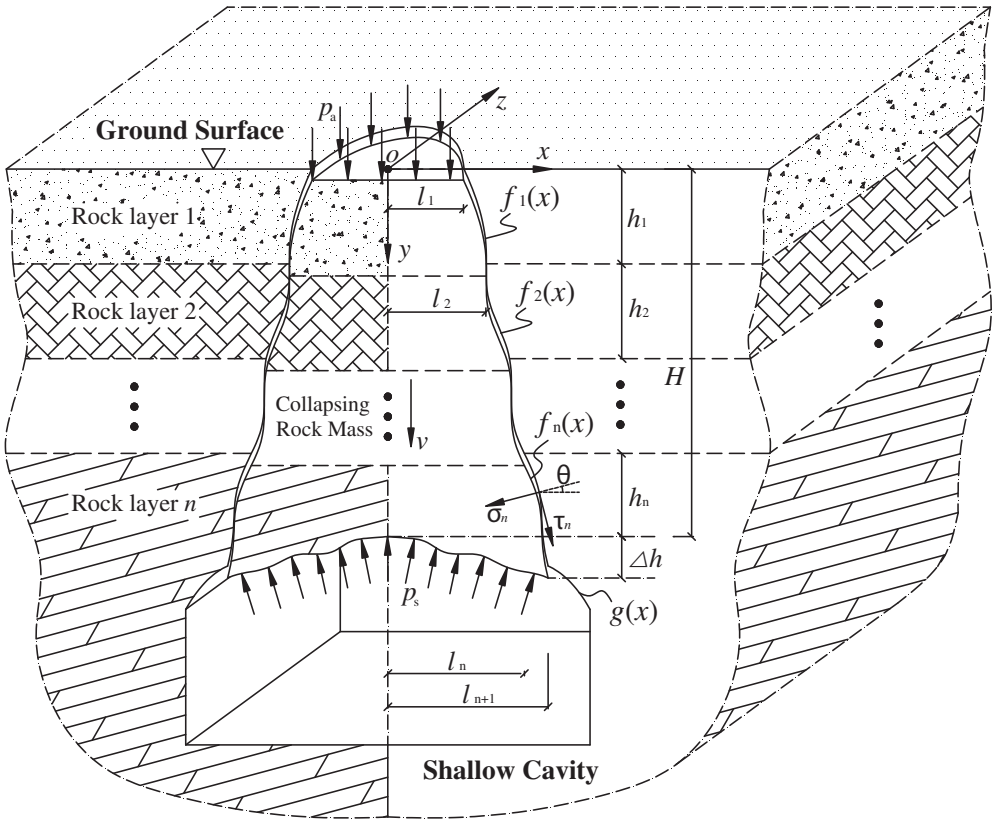

Figure 2: Three-dimensional axisymmetric collapse mechanism for a shallow cavity in layered rock strata

is the roof supporting pressure. The roof rock masses are assumed to be an ideal rigid-plastic medium, the collapsed rock masses are a rotational rigid block which is axisymmetric about the y-axis, and the downward velocity is v. The equation of collapse surface in roof rock layer i (i = 1, 2, …, n) is $f_i(x,z)$, and correspondingly $f_i(x)$ in plane $x-y$. The equation of cavity profile surface is $g(x,z)$, and correspondingly $g(x)$ in plane $x-y$. Practically, the spherical and rectangular cavity profiles are common, then the corresponding equations of $g(x)$ can be respectively given as follows:

$$g(x)=\begin{cases}-\sqrt{R^2-x^2}+H+R & \text{Spherical cavity}\\ H & \text{Rectangular cavity}\end{cases} \tag{3}$$

where R refers to the radius of a spherical cavity.

4 Three-Dimensional Upper Bound Limit Analysis of Roof Collapse for a Shallow Cavity

According to the three-dimensional axisymmetric velocity field in Fig. 2 and upper bound theorem, it is necessary to firstly calculate the internal energy dissipation rate and work rates of external forces in collapsing process. Wherein the internal energy dissipation occurs only at rock failure surfaces due to the above assumption that the roof rock masses are ideal rigid-plastic. Fraldi et al. [12] once assumed the rock failure surface as a thin deformation layer with certain thickness, and figured out the rate of internal energy dissipation in the thin layer based on traditional potential theory and Hoek-Brown strength criterion. Referring to the results by Fraldi et al. [12], we can obtain the rate of internal energy dissipation per unit volume corresponding to the collapse surfaces in n rock layers as follows:

$$\dot{D} = \sigma_n \dot{\epsilon}_n + \tau_n \dot{\gamma}_n = \left\{ \sum_{i=1}^{n} \left[-\sigma_{ti} + \sigma_{ci} (A_i B_i)^{1/(1-B_i)} \left(1 - B_i^{-1}\right) f'_i(x)^{1/(1-B_i)} \right] / \left[w_i \sqrt{1 + f'_i(x)^2} \right] \right\} \cdot v \tag{4}$$

where $\dot{\varepsilon}_n$ and $\dot{\gamma}_n$ are the normal strain rate and shear strain rate in plastic stage at the rock failure surface, which can be calculated based on Eq. (2); A_i, B_i, σ_{ti} and σ_{ci} (i = 1, 2, …, n) respectively refer to the empirical parameters, tensile strength, and compressive strength of rock mass in roof layer i; w_i (i = 1, 2, …, n) refers to the thickness of the thin deformation layer in rock layer i.

Integrating the Eq. (4) along the rock failure surfaces in n rock layers yields the total rate of internal energy dissipation:

$$\Omega_D = 2\pi \sum_{i=1}^{n} \int_{l_i}^{l_{i+1}} \left[-\sigma_{ti} x + \sigma_{ci} (A_i B_i)^{1/(1-B_i)} \left(1 - B_i^{-1}\right) x f'_i(x)^{1/(1-B_i)} \right] dx \cdot v \tag{5}$$

where l_i (i = 1, 2, …, n) is the failure width in layer i.

The work rate done by the weight of collapsed rock masses is:

$$W_\gamma = \left\{ \sum_{i=1}^{n} \pi \gamma_i l_i^2 h_i + 2\pi \sum_{i=1}^{n} \int_{l_i}^{l_{i+1}} \gamma_i \left[\sum_{j=1}^{i} h_j x - x f_i(x) \right] dx - \pi \gamma_n H l_{n+1}^2 + 2\pi \int_0^{l_{n+1}} \gamma_n x g(x) dx \right\} v \tag{6}$$

where h_i (i = 1, 2, …, n) is the thickness of layer i; Δh is the vertical distance from the bottom boundary of collapsed block to the central point of roof profile. If the roof profile is a plane, $\Delta h = 0$, whereas $\Delta h = R - \sqrt{R^2 - l_{n+1}^2}$ for a spherical surface.

The work rate of the roof supporting pressure is:

$$W_s = -2\pi \int_0^s \frac{p_s x}{\sqrt{1 + g'(x)^2}} ds \cdot v = -2\pi \int_0^{l_{n+1}} p_s x dx \cdot v = -\pi p_s l_{n+1}^2 v \tag{7}$$

where s refers to the arc length of the roof profile curve $g(x)$ in $(0, l_{n+1})$ range.

The work rate of the ground overload is:

$$W_a = \pi l_1^2 p_a v \tag{8}$$

On the basis of the internal energy dissipation rate and work rates of external forces in Eqs. (5)–(8), an objective function to obtain the true roof collapse mechanism can be built:

$$\Phi = \Omega_D + W_\gamma + W_s + W_a = \left\{ 2\pi \sum_{i=1}^{n} \int_{l_i}^{l_{i+1}} \Lambda_i[x, f_i(x), f'_i(x)] dx + \sum_{i=1}^{n} \pi \gamma_i l_i^2 h_i - \pi \gamma_n H l_{n+1}^2 + 2\pi \int_0^{l_{n+1}} \gamma_n x g(x) dx - \pi p_s l_{n+1}^2 + \pi l_1^2 p_a \right\} v \tag{9}$$

where $\Lambda_i[x, f_i(x), f'_i(x)]$ is:

$$\Lambda_i[x, f_i(x), f'_i(x)] = -\sigma_{ti} x + \sum_{j=1}^{i} \gamma_i h_j x + \sigma_{ci} (A_i B_i)^{1/(1-B_i)} \left(1 - B_i^{-1}\right) x f'_i(x)^{1/(1-B_i)} - \gamma_i x f_i(x) \tag{10}$$

Eq. (9) is a functional about x and $f_i(x)$, which indicates the magnitude of the total energy loss rate in the whole mechanism of Fig. 2. The curve equation $f_i(x)$ ($i = 1, 2, \ldots, n$) corresponding to the true roof collapse mechanism should enable Eq. (9) to obtain the extremum, which is a typical variation problem. Furtherly, the following Euler-Lagrange equation can be employed to solve this problem.

$$\frac{\partial \Lambda_i}{\partial f_i(x)} - \frac{\partial}{\partial x}\left(\frac{\partial \Lambda_i}{\partial f'_i(x)}\right) = 0 \tag{11}$$

Substituting Eq. (10) into Eq. (11) results:

$$-\gamma_i x + \sigma_{ci}(A_i B_i)^{1/(1-B_i)} B_i^{-1} f'_i(x)^{B_i/(1-B_i)} + \sigma_{ci}(A_i B_i)^{1/(1-B_i)}(1-B_i)^{-1} x f_i'(x)^{(2B_i-1)/(1-B_i)} f_i''(x) = 0 \tag{12}$$

A first integration of Eq. (12) gives:

$$f'_i(x) = \sigma_{ci}^{(B_i-1)/B_i} A_i^{-1/B_i} B_i^{-1}\left(\frac{\gamma_i}{2}x + \frac{C_i}{x}\right)^{(1-B_i)/B_i} \tag{13}$$

A further integration of Eq. (13) can give the collapse curve equation $f_i(x)$ in rock layer i. However, the calculation of Eq. (13) is quite complex, and it is difficult to figure out the analytical solution, which brings great inconveniences for roof stability analysis and support design in such strata. In view of this problem, Fig. 2 and the research findings of Yang et al. [18], Huang et al. [19], Guan et al. [20] and Wang et al. [31] can be referred to. Since the collapsed roof rock masses are assumed as a rotational rigid block, the collapse curve in each rock layer is symmetric to y-axis. From this, the first derivative of $f_i(x)$ is equal to 0 at the point $x = 0$, then the parameter C_i can be determined as 0, and Eq. (13) can be expressed as:

$$f'_i(x) = \xi_i B_i^{-1} x^{(1-B_i)/B_i} \tag{14}$$

where $\xi_i = (2\sigma_{ci}/\gamma_i)^{(B_i-1)/B_i} A_i^{-1/B_i}$.

Based on Eq. (14), we can obtain the general solution form of rock collapse curve equation $f_i(x)$ in layer i as follows:

$$f_i(x) = \xi_i x^{1/B_i} + D_i \tag{15}$$

where D_i refers to an integration constant. Rotating the curve $f_i(x)$ along y-axis can give the collapse surface equation $f_i(x,z)$ in rock layer i.

$$y = f_i(x,z) = \xi_i (x^2+z^2)^{1/2B_i} + D_i \tag{16}$$

By utilizing the geometrical relationships in Fig. 2, the rock collapse curve $f_i(x)$ meets:

$$\begin{cases} f_1(x)|_{x=l_1} = 0 \\ f_1(x)|_{x=l_2} = f_2(x)|_{x=l_2} = h_1 \\ f_2(x)|_{x=l_3} = f_3(x)|_{x=l_3} = h_1 + h_2 \\ \ldots \\ f_{n-1}(x)|_{x=l_n} = f_n(x)|_{x=l_n} = h_1 + h_2 + \ldots + h_{n-1} \\ f_n(x)|_{x=l_{n+1}} = g(x)|_{x=l_{n+1}} \end{cases} \tag{17}$$

By substituting Eq. (15) into Eq. (17), the integration constant D_i results:

$$\begin{cases} D_1 = -\xi_1 l_1^{1/B_1} \\ D_2 = h_1 - \xi_2 l_2^{1/B_2} \\ D_3 = h_1 + h_2 - \xi_3 l_3^{1/B_3} \\ \cdots \\ D_n = h_1 + h_2 + \ldots + h_{n-1} - \xi_n l_n^{1/B_n} \end{cases} \tag{18}$$

Furtherly, the following equations can be derived from Eq. (17):

$$\begin{cases} \xi_1 l_2^{1/B_1} - \xi_1 l_1^{1/B_1} = h_1 \\ \xi_2 l_3^{1/B_2} - \xi_2 l_2^{1/B_2} = h_2 \\ \xi_3 l_4^{1/B_3} - \xi_3 l_3^{1/B_3} = h_3 \\ \cdots \\ \xi_{n-1} l_n^{1/B_{n-1}} - \xi_{n-1} l_{n-1}^{1/B_{n-1}} = h_{n-1} \\ \xi_n l_{n+1}^{1/B_n} - \xi_n l_n^{1/B_n} = g(x)|_{x=l_{n+1}} - H + h_n \end{cases} \tag{19}$$

Eq. (19) contains n equations. However, it is still necessary to find another equation to calculate the collapse widths l_1-l_{n+1} of each layer in Fig. 2. Based on the upper bound theorem, the true roof collapse mechanism should enable the internal energy dissipation rate to be equal to the work rates of external forces. Namely that no energy loss occurs in the collapse mechanism in Fig. 2. Thus, by setting $\Phi = 0$ in Eq. (9) and substituting Eqs. (14)–(15) into it, the following equation can be obtained after simplification:

$$\begin{aligned} &\pi \sum_{i=1}^{n} \left\{ \left[-\sigma_{ti} + \sum_{j=1}^{i} \gamma_i h_j - \gamma_i D_i \right] (l_{i+1}^2 - l_i^2) + 2B_i (1+2B_i)^{-1} \right. \\ &\left. \left[\xi_i^{1/(1-B_i)} \sigma_{ci} A_i^{1/(1-B_i)} \left(1 - B_i^{-1}\right) - \gamma_i \xi_i \right] \left[l_{i+1}^{(1+2B_i)/B_i} - l_i^{(1+2B_i)/B_i} \right] \right\} + \sum_{i=1}^{n} \pi l_i^2 h_i \gamma_i \\ &- \pi \gamma_n H l_{n+1}^2 + 2\pi \int_0^{l_{n+1}} \gamma_n x g(x) dx - \pi p_s l_{n+1}^2 + \pi l_1^2 p_a = 0 \end{aligned} \tag{20}$$

By utilizing Eqs. (19)–(20), all collapse widths l_1~l_{n+1} can be solved. Thus the true collapse mechanism for shallow cavities in layered rock strata can be obtained. Accordingly, the overall weight of collapsed rock mass results:

$$P_G = \sum_{i=1}^{n} \pi \gamma_i l_i^2 h_i + 2\pi \sum_{i=1}^{n} \int_{l_i}^{l_{i+1}} \gamma_i \left[\sum_{j=1}^{i} h_j x - x f_i(x) \right] dx - \pi \gamma_n H l_{n+1}^2 + 2\pi \int_0^{l_{n+1}} \gamma_n x g(x) dx \tag{21}$$

5 Comparison Analysis of the Results

5.1 Comparison with Numerical Simulation Results

In order to evaluate the effectiveness of the proposed collapse mechanism in this paper, we select a rectangular cavity and a spherical cavity respectively as examples for investigation in this section. The FLAC-3D Software 3.0 is employed for numerical simulation analysis. This software is a finite difference program which has been widely applied in geotechnical engineering. By considering the shallow cavities being symmetrical in the vertical direction, the half is selected for consideration. The corresponding numerical calculation models are listed in Figs. 3 and 4. Wherein, the top of the models is the free boundary, the bottom boundaries are fixed with no horizontal and vertical displacement, and the side boundaries are fixed with no horizontal displacement. The buried depths of the two shallow cavities are

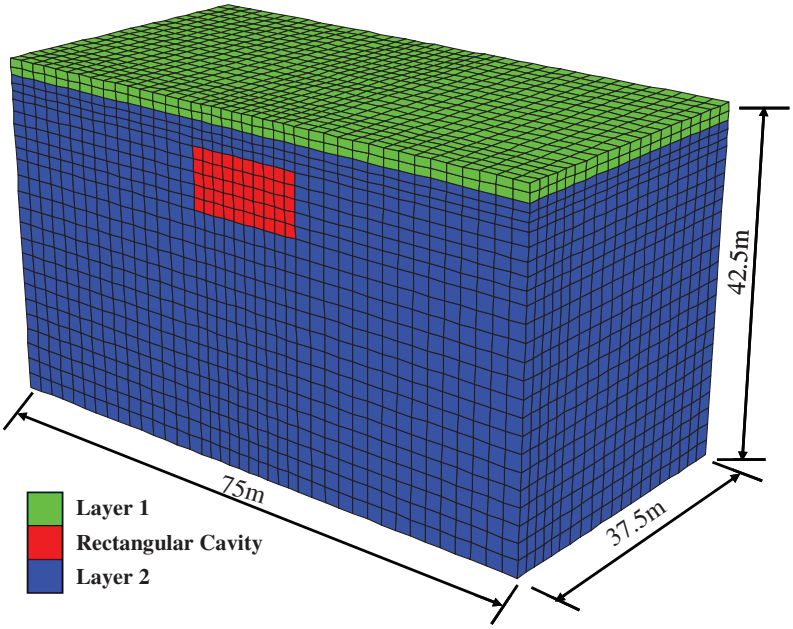

Figure 3: Numerical model for a rectangular cavity

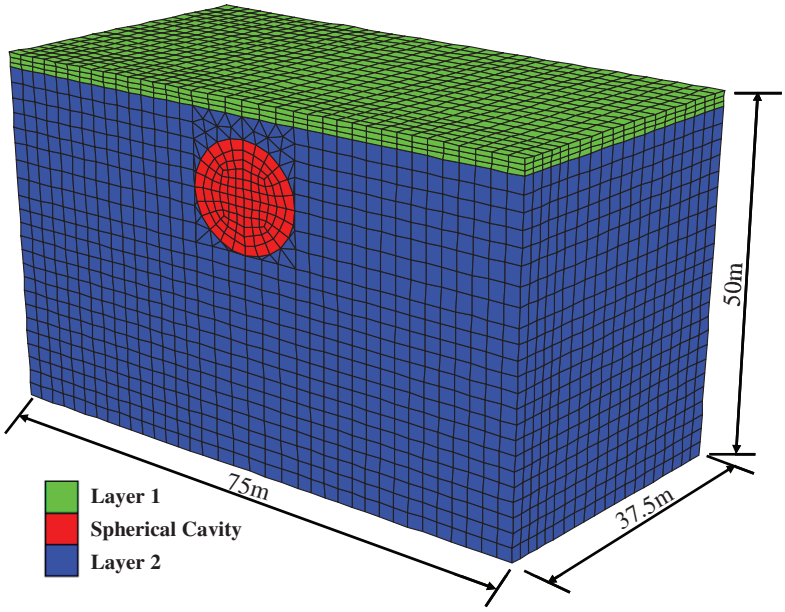

Figure 4: Numerical model for a spherical cavity

both 5 m. The roof surrounding rock masses are assumed comprising of two rock layers, and the upper layer and the lower layer are characterized as Layers 1 and 2 with thicknesses of 2 m, 3 m respectively.

The built-in Hoek-Brown constitutive model in FLAC-3D Software is applied to simulate the failure characteristics of roof surrounding rock masses. This model is defined through the form of principal stress [33–35] as follows:

$$\sigma_1 = \sigma_3 + \sigma_{ci}\left(m_b \frac{\sigma_3}{\sigma_{ci}} + s\right)^a \tag{22}$$

where σ_1 and σ_3 are the major and minor principal stresses, σ_{ci}, m_b, s and a are material constants. However, the adopted Hoek-Brown strength criterion in this paper is represented in terms of normal stress and shear stress in the Mohr plane $\sigma_n - \tau_n$, as listed in Eq. (1). The rock parameters in these two expressions are clear distinct, which also brings difficulties for comparison analysis in this paper. Fortunately, Hoek et al. [34] once proposed a linear regression analysis method to achieve this parameter transformation. Based on their method, the equivalent parameters A and B corresponding to the parameters m_b, s and a can be obtained. For example, Fraldi et al. [14] adopted this equivalent method to investigate the consistency between numerical simulation results and upper bound solution. With the same method, we adopt two sets of equivalent strength parameters for Layers 1 and 2 in the two numerical models respectively. Specifically, the parameters in the rectangular cavity model are: $m_{b1} = 3.1$, $s_1 = 0.035$, $a_1 = 0.62$, $\sigma_{c1} = 2.5$ MPa, and $\gamma_1 = 20$ kN/m^3 ($A_1 = 2/3$, $B_1 = 3/4$); $m_{b2} = 2.95$, $s_2 = 0.03$, $a_2 = 0.7$, $\sigma_{c2} = 2.5$ MPa, and $\gamma_2 = 19$ kN/m^3 ($A_2 = 2/3$, $B_2 = 4/5$). The parameters in the spherical cavity model are: $m_{b1} = 0.082$, $s_1 = 0.00042$, $a_1 = 0.522$, $\sigma_{c1} = 0.8$ MPa, and $\gamma_1 = 20$ kN/m^3 ($A_1 = 0.132$, $B_1 = 0.593$); $m_{b2} = 0.41$, $s_2 = 0.00042$, $a_2 = 0.522$, $\sigma_{c2} = 1.0$ MPa, and $\gamma_2 = 23$ kN/m^3 ($A_2 = 0.283$, $B_2 = 0.641$).

In the numerical simulation process, after the initial equilibrium of ground stress is implemented within the models, the shallow cavities are wholly excavated at a time. It should be noted that the FLAC-3D Software is a finite difference program based on continuum mechanics, and it may be relatively difficulty to reflect the collapse process of roof rock masses intuitively and vividly, compared with the discrete element method. Thus, we just analyze the deformation characteristics of the cavity roof to estimate the collapse pattern. Moreover, since the proposed theoretical model and the numerical model are all symmetrical with respect to y-axis, we just present the contours of vertical displacement in roof surrounding rock masses in plane x-y, as shown in Figs. 5 and 6. The collapse range results by the analytical method are also plotted in Figs. 5 and 6. It can be found that the results by the two different methods are basically identical in both the rectangular cavity model and the spherical cavity model, which indicates that the proposed method in this paper is valid to predict the collapse range of shallow cavities in layered strata.

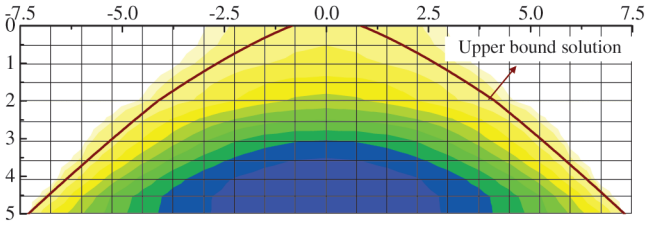

Figure 5: Contour of vertical displacement for the rectangular cavity

5.2 Comparison with Extant Research Results

As stated in the literature review in Section 1, the stfigability of tunnel roof has been the object of many works in recent years. But the collapse characteristics for a shallow rock cavity in layered strata have not been well investigated. In order to further evaluating the validity of the proposed method in this paper, the research of Qin et al. [26] is introduced for comparison in this section. In their works, a three-dimensional progressive collapse mechanism for a deep rectangular tunnel in partly weathered stratified rock strata was proposed. By comparing the mechanism of Qin et al. [26] and it in this paper, we may set the collapse width l_1 at the ground

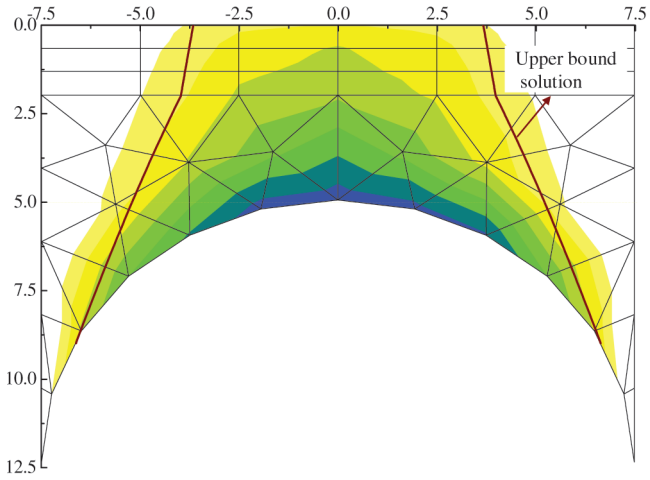

Figure 6: Contour of vertical displacement for the spherical cavity

surface in Fig. 2 to be zero. By doing so, the cavity roof in Fig. 2 can form an arch bearing structure inside and present the collapse characteristics of deep cavities. Then the proposed mechanism can be converted into the mechanism of Qin et al. [26]. Furtherly, under this condition, Tab. 1 lists several comparison results of collapse range under these two mechanisms. Wherein, it should be noted that when the width l_1 is set to be zero in Fig. 2, the height H of the collapse range is unknown and need to be solved. As can be seen in Tab. 1, the collapse range calculated by these two methods is almost identical, which shows good validity of the method in this paper.

Table 1: Comparisons with the three-dimensional mechanism by Qin et al. [26]

A_1	A_2	B_1	B_2	σ_{c1} /MPa	σ_{c2} /MPa	γ_1 /kN·m^{-3}	γ_2 /kN·m^{-3}	$\frac{h_1}{H}$	The mechanism by Qin et al. [26]			The mechanism by this paper		
									l_2/m	l_3/m	H/m	l_2/m	l_3/m	H/m
0.3	0.6	0.7	0.6	1	1.5	20	25	0.5	1.7891	6.2371	3.5625	1.7891	6.2371	3.5625
0.3	0.3	0.7	0.6	1	1.5	20	25	0.5	1.4531	2.9862	2.6466	1.4531	2.9862	2.6466
0.3	0.6	0.7	0.7	1	1.5	20	25	0.5	1.5007	3.8981	2.7714	1.5007	3.8981	2.7714
0.3	0.6	0.7	0.6	1	1	20	25	0.5	1.3406	4.2101	2.3590	1.3406	4.2101	2.3590
0.3	0.6	0.7	0.6	1	1.5	20	25	0.1	0.4414	6.5280	2.4124	0.4414	6.5280	2.4124
0.3	0.6	0.7	0.6	1	1.5	20	20	0.5	2.1017	7.7675	4.4842	2.1017	7.7675	4.4842

Further, we also chose the two-dimensional collapse mechanism for a shallow circular tunnel in layered rock strata by Yang et al. [29] as a reference for comparison. By using the same parameters, the calculation results of collapse range by the proposed three-dimensional mechanism in this paper and that by Yang et al. [29] are listed in Tab. 2. Wherein, the adoptive parameters are $R = 5$ m, $H = 4$ m, $\sigma_{c1} = \sigma_{c2} = 0.5$ MPa, $\sigma_{t1} = \sigma_{t2} = \sigma_{c1}/100$, $\gamma_1 = \gamma_2 = 17.5$ kN/m^3, $p_s = 40$ kPa, and $p_a = 0$ kPa respectively.

It can be found from Tab. 2 that the results computed by the two-dimensional and three-dimensional collapse mechanisms are significantly different. Particularly, the widths of collapse rock masses by three-dimensional mechanism are larger than those by two-dimensional mechanism in whole, which is similar to the research findings for deep cavities by Yang et al. [18]. Namely, the results by the two-dimensional

Table 2: Comparisons with the two-dimensional mechanism by Yang et al. [29]

A_1	A_2	B_1	B_2	Two-dimensional mechanism by Yang et al. [29]			Three-dimensional mechanism by this paper		
				l_1/m	l_2/m	l_3/m	l_1/m	l_2/m	l_3/m
0.05	0.10	0.8	0.7	1.32	1.49	1.64	1.61	1.70	1.97
0.10	0.15	0.8	0.7	1.22	1.56	1.87	2.96	3.14	3.71
0.15	0.20	0.9	0.8	1.51	1.90	2.35	2.46	2.77	3.53
0.20	0.15	0.7	0.8	0.43	1.32	1.85	2.39	2.92	3.44
0.30	0.10	0.7	0.8	0.16	1.50	1.88	1.80	2.79	3.08

mechanism tend to underestimate the potential collapse range, while those by the three-dimensional mechanism are relatively safer for engineering designing actually. Thus, in order to guarantee the roof safety of shallow cavities, the three-dimensional collapse case should be paid much care in real scenarios.

5.3 Comparison Analysis of Roof Collapse Range under Varying Parameters

In order to investigate the change laws of the three-dimensional collapse mechanisms under varying mechanical parameters, the rectangular and spherical cavities in two-layered strata are taken for consideration respectively.

(1) Rectangular cavity

The burial depth of the shallow rectangular cavity is set 5 m, the thickness of rock layer 1 is 2.5 m, and then the equation of roof border is $g(x) = 5$. Tab. 3 presents the corresponding results of roof collapse range regarding varying parameters.

The results in Tab. 3 show that with the increase of the ground overload, parameter B, and unit weight of the rock Layers 1 and 2, the widths of roof collapsing rock masses tend to decrease, while increase as the supporting pressure, empirical parameter A, compressive strength, and tensile strength of the two rock layers increase. Particularly, compared with other parameters, the ground overload, supporting pressure, and parameters A, B may significantly affect the magnitude of collapse range, which should be pad much care in actual engineering. Wherein, the parameters A, B in Hoek-Brown criterion represent the quality of rock masses. From an engineering standpoint, several recommendations can be given as follows to avoid the collapse risk of shallow cavities:

a) During the excavation or operation period, all kinds of facilities with great weight on ground surface should be removed in good time to mitigate the adverse influence of additional load. Moreover, the ground traffic vibration effect on shallow cavity should also be paid much care.
b) Sufficient supporting pressure is the premise to ensure the long-term stability of shallow cavities [37,38]. The support components with high-strength or high-rigidity should be encouraged, especially when the shallow cavities pass through soft or weak strata.
c) The stratified characteristics of rock strata should be paid much care in cavity support design and excavation process. For the soft or weak rock layers, the techniques such as advanced pipe grouting, bolt grouting, etc., can be employed to reinforce the strata. Then the strength and integrity of rock masses can be effectively enhanced.

Table 3: Comparisons of collapse range for rectangular cavity under varying parameters

A_1	B_1	γ_1 /kN·m^{-3}	σ_{c1} /MPa	σ_{t1} /MPa	A_2	B_2	γ_2 /kN·m^{-3}	σ_{c2} /MPa	σ_{t2} /MPa	p_s /kPa	p_a /kPa	l_1 /m	l_2 /m	l_3 /m
0.1	0.8	18	0.4	0.004	0.2	0.7	20	0.6	0.006	50	0	2.73	2.95	3.56
0.1	0.8	18	0.4	0.004	0.2	0.7	20	0.6	0.006	50	20	1.79	2.04	2.74
0.1	0.8	18	0.4	0.004	0.2	0.7	20	0.6	0.006	50	40	1.41	1.67	2.42
0.1	0.8	18	0.4	0.004	0.2	0.7	20	0.6	0.006	20	20	0.41	0.74	1.68
0.1	0.8	18	0.4	0.004	0.2	0.7	20	0.6	0.006	35	20	1.02	1.30	2.11
0.1	0.8	18	0.4	0.004	0.2	0.7	20	0.6	0.006	65	20	3.10	3.32	3.90
0.2	0.8	18	0.4	0.004	0.3	0.7	20	0.6	0.006	50	20	2.73	3.26	4.28
0.3	0.8	18	0.4	0.004	0.4	0.7	20	0.6	0.006	50	20	3.67	4.48	5.83
0.4	0.8	18	0.4	0.004	0.5	0.7	20	0.6	0.006	50	20	4.62	5.71	7.39
0.1	0.6	18	0.4	0.004	0.2	0.5	20	0.6	0.006	50	20	3.57	3.74	4.47
0.1	0.7	18	0.4	0.004	0.2	0.6	20	0.6	0.006	50	20	2.51	2.73	3.47
0.1	0.9	18	0.4	0.004	0.2	0.8	20	0.6	0.006	50	20	1.28	1.54	2.18
0.1	0.8	18	0.2	0.004	0.2	0.7	20	0.4	0.006	50	20	1.58	1.80	2.42
0.1	0.8	18	0.6	0.004	0.2	0.7	20	0.8	0.006	50	20	1.95	2.22	2.98
0.1	0.8	18	0.8	0.004	0.2	0.7	20	1.0	0.006	50	20	2.09	2.37	3.19
0.1	0.8	18	0.4	0.002	0.2	0.7	20	0.6	0.004	50	20	1.72	1.97	2.68
0.1	0.8	18	0.4	0.006	0.2	0.7	20	0.6	0.008	50	20	1.86	2.11	2.80
0.1	0.8	18	0.4	0.008	0.2	0.7	20	0.6	0.010	50	20	1.93	2.18	2.86
0.1	0.8	16	0.4	0.004	0.2	0.7	18	0.6	0.006	50	20	2.20	2.45	3.13
0.1	0.8	20	0.4	0.004	0.2	0.7	22	0.6	0.006	50	20	1.49	1.74	2.45
0.1	0.8	22	0.4	0.004	0.2	0.7	24	0.6	0.006	50	20	1.27	1.52	2.24

(2) Spherical cavity

Similarly, the roof failure surfaces of the shallow spherical cavity in plane x-y under varying burial depths, thicknesses of rock layers and excavation radiuses are plotted in Figs. 7–9. Wherein, the values of strength parameters in the upper and lower rock layers are $A_1 = 0.1$, $B_1 = 0.8$, $\gamma_1 = 18$ kN/m^3, $\sigma_{c1} = 0.4$ MPa, $\sigma_{t1} = \sigma_{c1}/100$, $A_2 = 0.15$, $B_2 = 0.7$, $\gamma_2 = 20$ kN/m^3, $\sigma_{c2} = 0.6$ MPa, and $\sigma_{t2} = \sigma_{c2}/100$ respectively. The supporting pressure and ground overload are $p_s = 50$ kPa, $p_a = 0$ kPa.

From the Figs. 7–9, it can be seen that with an increase in the burial depth of the spherical cavity, the heights of the collapsing rock masses increase, whereas the widths decrease. This means there must be a critical depth at which the collapse width at the top reaches to zero and the collapse characteristics of the deep cavity may present. When the burial depth is certain, the layered characteristics of the cavity roof also have significant influence on the collapse range. Specifically, the magnitude of the collapse region decreases as the thickness of upper rock layer, due to varying rock parameters in the upper and lower layers. Besides, as for the spherical cavity, the collapse range is also affected by the excavation radius. But the effect of cavity radius on it is not obvious, which is identical to the analytical results by Qin et al. [21,22]. Thus, in practical engineering, the influences, such as burial depth, layered characteristics and excavation size, should also be paid much care in cavity support design.

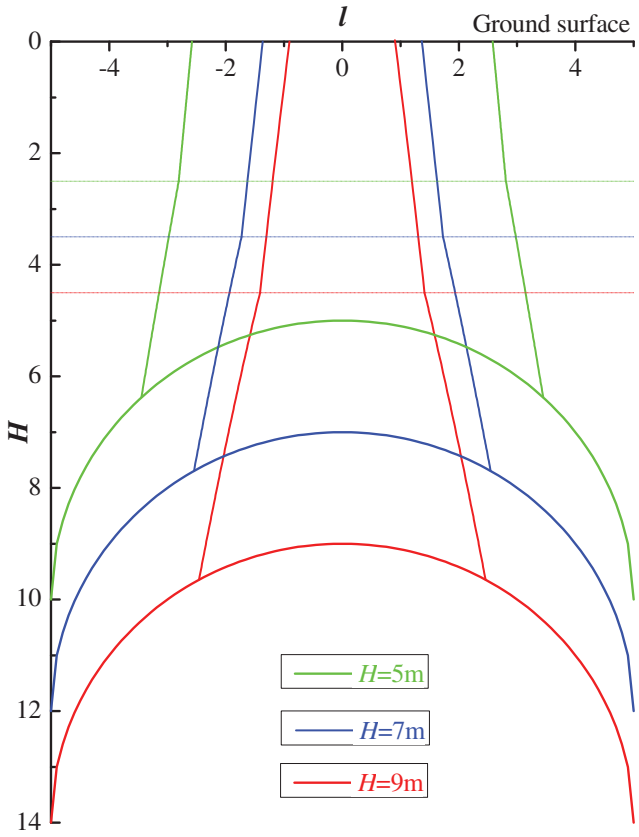

Figure 7: Effect of varying burial depths on roof collapse curve

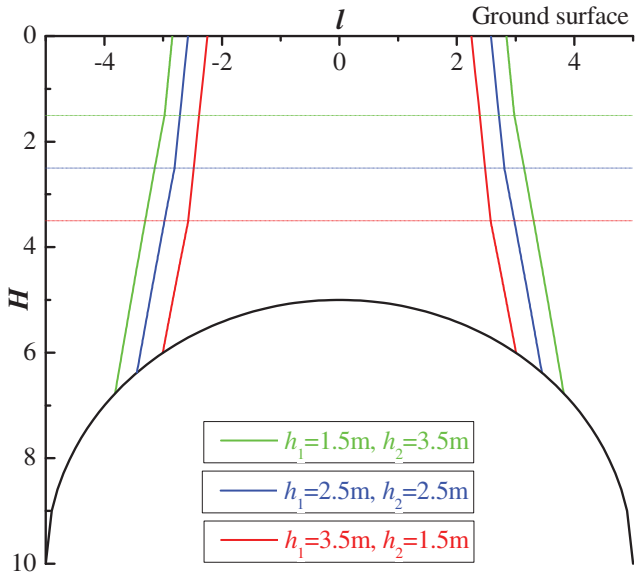

Figure 8: Effect of varying thicknesses of rock layer on roof collapse curve

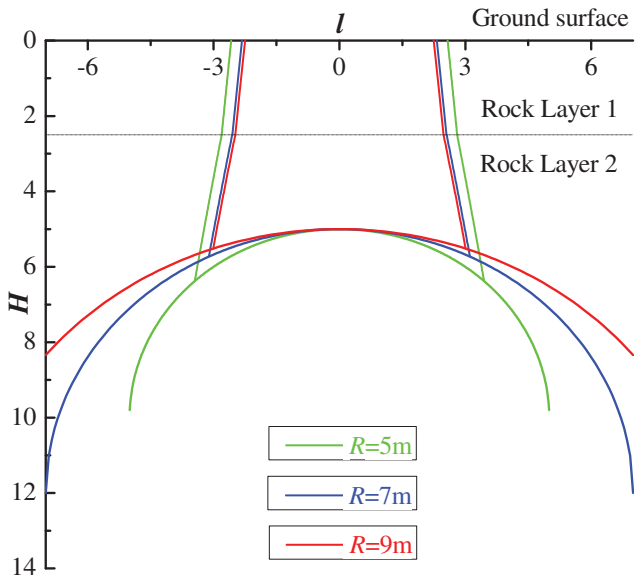

Figure 9: Effect of varying excavation radiuses on roof collapse curve

6 Conclusions

(1) This paper presents a three-dimensional axisymmetric collapse mechanism for a shallow cavity with arbitrary profiles in layered rock strata. The analytical solutions of roof collapse surfaces and the corresponding weight of collapsing rock masses are derived on the basis of the Hoek-Brown strength criterion and upper bound theorem. The proposed method in this paper can be utilized to predict the potential roof collapse range in layered rock strata.

(2) The results by the presented method are well consistent with the numerical simulation results and extant research results, which validate the effectiveness of the proposed method. In addition, the widths of collapse rock masses by three-dimensional mechanism are larger than those by two-dimensional mechanism in whole. The two-dimensional mechanism tends to underestimate the potential collapse range of shallow cavity, while the three-dimensional mechanism is relatively safer for engineering designing actually.

(3) The change laws of the collapse range under varying parameters are obtained for the presence of rectangular and spherical cavities. It is found that the collapse range is positively related to supporting pressure, parameter A, compressive strength, and tensile strength of rock layer, but negatively related to ground overload, parameter B, and unit weight. Further, the effect of ground overload, supporting pressure and parameters A, B on the collapse range is more significant. Particularly, we observe that with an increase in the burial depth of the spherical cavity, the heights of the collapsing rock mass increase, whereas the widths decrease. Besides, the collapse range decreases as the thickness of the upper rock layer and excavation radius increase.

Acknowledgement: The authors express sincere appreciation to the reviewers for their valuable comments and suggestions, which improved the paper much.

Funding Statement: This research was funded by National Natural Science Foundation of China (Nos. 51704177, 51809159), A Project of Shandong Province Higher Educational Science and Technology Program (No. J16LG04), Open Research Fund of State Key Laboratory of Geomechanics and Geotechnical Engineering (No. Z018005), Shandong Co-Innovation Center for Disaster Prevention and

Mitigation of Civil Structures (No. XTP201911), and the Doctoral Research Fund of Shandong Jianzhu University (No. XNBS1501).

Conflicts of Interest: The authors declare that they have no conflicts of interest to report regarding the present study.

References

1. Leca, E., Dormieux, L. (1990). Upper and lower bound solutions for the face stability of shallow circular tunnels in frictional material. *Geotechnique, 40(5),* 581–606. DOI 10.1680/geot.1990.40.4.581.
2. Lee, I. M., Nam, S. W. (2001). The study of seepage forces acting on the tunnel lining and tunnel face in shallow tunnels. *Tunnelling and Underground Space Technology, 16(1),* 31–40. DOI 10.1016/S0886-7798(01)00028-1.
3. Pinyol, N. M., Alonso, E. E. (2011). Design of micropiles for tunnel face reinforcement: undrained upper bound solution. *Journal of Geotechnical and Geoenvironmental Engineering, 138(1),* 89–99. DOI 10.1061/(ASCE) GT.1943-5606.0000562.
4. Mollon, G., Dias, D., Soubra, A. H. (2013). Continuous velocity fields for collapse and blowout of a pressurized tunnel face in purely cohesive soil. *International Journal for Numerical and Analytical Methods in Geomechanics, 37(13),* 2061–2083. DOI 10.1002/nag.2121.
5. Tang, X. W., Liu, W., Albers, B., Savidis, S. (2014). Upper bound analysis of tunnel face stability in layered soils. *Acta Geotechnica, 9(4),* 661–671. DOI 10.1007/s11440-013-0256-1.
6. Zhang, C., Han, K., Zhang, D. (2015). Face stability analysis of shallow circular tunnels in cohesive-frictional soils. *Tunnelling and Underground Space Technology, 50,* 345–357. DOI 10.1016/j.tust.2015.08.007.
7. Han, K., Zhang, C., Zhang, D. (2016). Upper-bound solutions for the face stability of a shield tunnel in multilayered cohesive-frictional soils. *Computers and Geotechnics, 79,* 1–9. DOI 10.1016/j.compgeo.2016.05.018.
8. Huang, M., Tang, Z., Zhou, W., Yuan, J. (2018). Upper bound solutions for face stability of circular tunnels in non-homogeneous and anisotropic clays. *Computers and Geotechnics, 98,* 189–196. DOI 10.1016/j.compgeo.2018.02.015.
9. Zhang, F., Gao, Y., Wu, Y., Wang, Z. (2018). Face stability analysis of large-diameter slurry shield-driven tunnels with linearly increasing undrained strength. *Tunnelling and Underground Space Technology, 78,* 178–187. DOI 10.1016/j.tust.2018.04.018.
10. Li, W., Zhang, C., Zhu, W., Zhang, D. (2019). Upper-bound solutions for the face stability of a non-circular NATM tunnel in clays with a linearly increasing undrained shear strength with depth. *Computers and Geotechnics, 114,* 103136. DOI 10.1016/j.compgeo.2019.103136.
11. Li, W., Zhang, C. P. (2019). Face stability analysis for a shield tunnel in anisotropic sands. *International Journal of Geomechanics, 20(5),* 04020043. DOI 10.1061/(ASCE)GM.1943-5622.0001666
12. Fraldi, M., Guarracino, F. (2009). Limit analysis of collapse mechanisms in cavities and tunnels according to the Hoek-Brown failure criterion. *International Journal of Rock Mechanics and Mining Sciences, 46(4),* 665–673. DOI 10.1016/j.ijrmms.2008.09.014.
13. Fraldi, M., Guarracino, F. (2010). Analytical solutions for collapse mechanisms in tunnels with arbitrary cross sections. *International Journal of Solids and Structures, 47(2),* 216–223. DOI 10.1016/j.ijsolstr.2009.09.028.
14. Fraldi, M., Guarracino, F. (2011). Evaluation of impending collapse in circular tunnels by analytical and numerical approaches. *Tunnelling and Underground Space Technology, 26(4),* 507–516. DOI 10.1016/j.tust.2011.03.003.
15. Fraldi, M., Cavuoto, R., Cutolo, A., Guarracino, F. (2019). Stability of tunnels according to depth and variability of rock mass parameters. *International Journal of Rock Mechanics and Mining Sciences, 119,* 222–229. DOI 10.1016/j.ijrmms.2019.05.001.
16. Huang, F., Yang, X. L. (2011). Upper bound limit analysis of collapse shape for circular tunnel subjected to pore pressure based on the Hoek-Brown failure criterion. *Tunnelling and Underground Space Technology, 26(5),* 614–618. DOI 10.1016/j.tust.2011.04.002.

17. Zhang, C. P., Han, K. H., Fang, Q., Zhang, D. L. (2014). Functional catastrophe analysis of collapse mechanisms for deep tunnels based on the Hoek-Brown failure criterion. *Journal of Zhejiang University Science A, 15(9),* 723–731. DOI 10.1631/jzus.A1400014.
18. Yang, X. L., Huang, F. (2013). Three-dimensional failure mechanism of a rectangular cavity in a Hoek-Brown rock medium. *International Journal of Rock Mechanics and Mining Sciences, 61,* 189–195. DOI 10.1016/j.ijrmms.2013.02.014.
19. Huang, F., Yang, X. L., Ling, T. H. (2014). Prediction of collapsing region above deep spherical cavity roof under axis-symmetrical conditions. *Rock Mechanics and Rock Engineering, 47(4),* 1511–1516. DOI 10.1007/s00603-013-0455-y.
20. Guan, K., Zhu, W. C., Niu, L. L., Wang, Q. Y. (2017). Three-dimensional upper bound limit analysis of supported cavity roof with arbitrary profile in Hoek-Brown rock mass. *Tunnelling and Underground Space Technology, 69,* 147–154. DOI 10.1016/j.tust.2017.06.016.
21. Qin, C. B., Yang, X. L., Pan, Q. J., Sun, Z. B., Wang, L. L. et al. (2015). Upper bound analysis of progressive failure mechanism of tunnel roofs in partly weathered stratified Hoek-Brown rock masses. *International Journal of Rock Mechanics and Mining Sciences, 74,* 157–162. DOI 10.1016/j.ijrmms.2014.10.002.
22. Qin, C. B., Chian, S. C., Yang, X. L., Du, D. C. (2015). 2D and 3D limit analysis of progressive collapse mechanism for deep-buried tunnels under the condition of varying water table. *International Journal of Rock Mechanics and Mining Sciences, 80,* 255–264. DOI 10.1016/j.ijrmms.2015.09.024.
23. Yang, X. L., Zhou, T., Li, W. T. (2018). Reliability analysis of tunnel roof in layered Hoek-Brown rock masses. *Computers and Geotechnics, 104,* 302–309. DOI 10.1016/j.compgeo.2017.12.007.
24. Yang, X. L., Yao, C. (2018). Stability of tunnel roof in nonhomogeneous soils. *International Journal of Geomechanics, 18(3),* 06018002. DOI 10.1061/(ASCE)GM.1943-5622.0001104.
25. Yang, X. L., Yao, C. (2017). Axisymmetric failure mechanism of a deep cavity in layered soils subjected to pore pressure. *International Journal of Geomechanics, 17(8),* 04017031. DOI 10.1061/(ASCE)GM.1943-5622.0000911.
26. Qin, C. B., Chian, S. C., Yang, X. L. (2017). 3D limit analysis of progressive collapse in partly weathered Hoek-Brown rock banks. *International Journal of Geomechanics, 17(7),* 04017011. DOI 10.1061/(ASCE)GM.1943-5622.0000885.
27. Qin, C., Chian, S. C. (2018). Revisiting crown stability of tunnels deeply buried in non-uniform rock surrounds. *Tunnelling and Underground Space Technology, 73,* 154–161. DOI 10.1016/j.tust.2017.12.006.
28. Yang, X. L., Huang, F. (2011). Collapse mechanism of shallow tunnel based on nonlinear Hoek-Brown failure criterion. *Tunnelling and Underground Space Technology, 26(6),* 686–691. DOI 10.1016/j.tust.2011.05.008.
29. Yang, X. L., Li, K. F. (2017). Roof collapse of shallow tunnel in layered Hoek-Brown rock media. *Geomechanics and Engineering, 11(6),* 867–877. DOI 10.12989/gae.2016.11.6.867.
30. Wang, H. T., Wang, L. G., Li, S. C., Wang, Q., Liu, P. et al. (2019). Roof collapse mechanisms for a shallow tunnel in two-layer rock strata incorporating the influence of groundwater. *Engineering Failure Analysis, 98,* 215–227. DOI 10.1016/j.engfailanal.2019.01.062.
31. Wang, H. T., Liu, P., Liu, C., Zhang, X., Yang, Y. et al. (2019). Three-dimensional upper bound limit analysis on the collapse of shallow soil tunnels considering roof stratification and pore water pressure. *Mathematical Problems in Engineering,* 1–15. DOI 10.1155/2019/8164702.
32. Lyu, C., Zeng, Z. Q. (2019). Upper bound limit analysis of unsymmetrical progressive collapse of shallow tunnels in inclined rock stratum. *Computers and Geotechnics, 116,* 103199. DOI 10.1016/j.compgeo.2019.103199.
33. Hoek, E., Brown, E. T. (1980). Underground excavations in rock. *Institution of Mining and Metallurgy,* London, Taylor & Francis.
34. Hoek, E., Brown, E. T. (1997). Practical estimates of rock mass strength. *International Journal of Rock Mechanics and Mining Sciences, 34(8),* 1165–1186. DOI 10.1016/S1365-1609(97)80069-X.
35. Hoek, E., Marinos, P. (2007). A brief history of the development of the Hoek-Brown failure criterion. *Journal of Soils and Rocks, 2,* 1–11.
36. Chen, W. F. (1974). *Limit analysis and soil plasticity.* Elsevier, Amsterdam, Netherlands.

37. Li, W. T., Yang, N., Mei, Y. C., Zhang, Y. H., Wang, L. et al. (2020). Experimental investigation of the compression-bending property of the casing joints in a concrete filled steel tubular supporting arch for tunnel engineering. *Tunnelling and Underground Space Technology, 96,* 103184. DOI 10.1016/j.tust.2019.103184.
38. Wang, H. T., Li, S. C., Wang, Q., Wang, D. C., Li, W. T. et al. (2019). Investigating the supporting effect of rock bolts in varying anchoring methods in a tunnel. *Geomechanics and Engineering, 19(6),* 485–498.